

Received 17 November 2025, accepted 13 December 2025, date of publication 17 December 2025,  
date of current version 7 January 2026.

Digital Object Identifier 10.1109/ACCESS.2025.3645434

## RESEARCH ARTICLE

# High-Resolution Multi-Target Angle Estimation for IoT-Enabled Drone Detection Using Adaptive Monopulse Beamforming

HUIJEA PARK<sup>1</sup>, JIWON KIM<sup>1</sup>, JAEHYUN PARK<sup>1</sup>, (Member, IEEE), JAE CHEOL PARK<sup>2</sup>,  
AND JUNGICK MOON<sup>2</sup>, (Member, IEEE)

<sup>1</sup>Department of Electronic Engineering, Pukyong National University, Busan 48513, South Korea

<sup>2</sup>Electronics and Telecommunications Research Institute (ETRI), Daejeon 34129, South Korea

Corresponding author: Jaehyun Park (jaehyun@pknu.ac.kr)

This work was supported in part by the National Research Foundation of Korea (NRF) Grant funded by Korea Government (MSIT) under Grant RS-2023-00241706 and was also supported by Institute of Information and communications Technology Planning and Evaluation (IITP) grant funded by the Korea government (MSIT) (No.RS-2024-00398981, Development of multi-meter level radio beam wireless charging technology based on millimeter waves).

**ABSTRACT** This paper presents an iterative monopulse beamforming method for accurate angle-of-arrival (AoA) estimation of multiple closely spaced targets in IoT-enabled frequency-modulated continuous wave (FMCW) multiple-input multiple-output (MIMO) radar systems, with a specific focus on drone detection and tracking applications. As the Internet of Things (IoT) continues to expand, the need for reliable and efficient drone detection systems has become increasingly critical for security, surveillance, and airspace management. Unlike conventional monopulse beamforming that suffers from limited resolution and interference in multi-target environments, the proposed method formulates a constrained convex optimization problem to design sum and difference beams with precise control over mainlobe gain, sidelobe suppression, and monopulse slope. To further improve robustness against closely spaced targets, we introduce a nulling method followed by an iterative refinement algorithm that alternately updates beamformers while incorporating interference suppression constraints. Additionally, we develop a low-complexity iterative nulling algorithm based on orthogonal projection with slope and bias calibration to reduce computational complexity, making it suitable for resource-constrained IoT devices. Both computer simulations and laboratory experiments using commercial radar modules demonstrate that our proposed methods significantly outperform conventional monopulse techniques, particularly when targets are closely spaced. The iterative nulling approach achieves up to 70% reduction in mean square error (MSE) compared to conventional methods across various signal-to-noise ratio (SNR) levels, making it highly suitable for IoT-based drone detection and tracking applications.

**INDEX TERMS** IoT-enabled radar systems, drone detection and tracking, Iterative monopulse beamforming, angle-of-arrival (AoA) estimation, FMCW MIMO radar.

## I. INTRODUCTION

The rapid proliferation of drones in various applications, from delivery services to surveillance and recreational use, has created an urgent need for reliable detection and tracking systems in the Internet of Things (IoT) ecosystem [1]. This challenge is particularly critical in urban environments where multiple drones may operate simultaneously, requiring

high-resolution spatial awareness and accurate angle estimation capabilities. IoT-enabled radar systems, especially those based on frequency-modulated continuous wave (FMCW) multiple-input multiple-output (MIMO) technology, have emerged as promising solutions for this challenge due to their ability to provide precise spatial information while being cost-effective and energy-efficient [2].

The integration of radar systems into the IoT framework presents unique opportunities and challenges [3], [4]. On one hand, it enables seamless connectivity and data sharing

The associate editor coordinating the review of this manuscript and approving it for publication was Cheng Hu<sup>1</sup>.

across the IoT network, facilitating comprehensive drone monitoring and management [1], [4]. On the other hand, it requires sophisticated signal processing techniques that can operate efficiently within the constraints of IoT devices, such as limited computational resources and power consumption [5]. This dual requirement makes the development of efficient angle estimation algorithms crucial for the success of IoT-based drone detection systems.

To address the Angle-of-Arrival (AoA) estimation challenge in IoT-enabled radar systems, several signal processing techniques have been developed [6], [7], [8]. The multiple signal classification (MUSIC) algorithm offers high-resolution angle estimation but requires extensive signal samples and computationally intensive eigenvalue decomposition [9], [10], [11], [12]. To exploit the multi-dimensional structure of array measurements, tensor-based AoA estimation methods have been explored [13], [14], [15]. These state-of-the-art techniques, which can jointly estimate parameters [13], [15], [16], are powerful but are primarily designed for different system scales and applications. They typically target large-scale systems such as Massive MIMO or Integrated Sensing and Communication (ISAC) platforms, which rely on large arrays and complex processing of large data cubes (e.g., tensor decomposition), often implying higher latency. In contrast, our work is specifically tailored for resource-constrained IoT devices. We focus on a model-based, low-latency approach (capable of operating on a single snapshot) for a dedicated real-time tracking application, offering a practical and computationally efficient alternative for this specific domain.

While maximum likelihood methods can effectively estimate target angles with limited signal samples, they require nonlinear signal processing with high computational complexity [17], which may not be practical for IoT applications. In addition to traditional high-resolution algorithms like MUSIC, recent advances have seen the successful application of sparse recovery and compressed sensing (CS) techniques to the AoA estimation problem [18], [19], [20], [21]. These methods can achieve superior resolution by exploiting the inherent sparsity of targets in the spatial domain. However, they often rely on the assumption of a static scene to construct the measurement matrix and can involve computationally intensive convex optimization or iterative greedy algorithms. In [22], [23], and [24], the data-driven deep-learning (DL)-based approaches have been developed to estimate AoA of targets. In [22], a deep convolutional neural network (CNN) is exploited for AoA estimation and, to reduce the complexity in the estimation of multiple target AoAs, the neural network architecture in [22] consists of multiple sub-networks, each supporting the subregion of the azimuth angle range. In [23], an unsupervised learning strategy is proposed for the AoA estimation. We note that these DL-based approaches depend on large training datasets, which contrasts with our model-based approach that does not require training. In addition, these may not be ideal for resource-constrained IoT devices that require the tracking of dynamic targets in real-time. Our proposed approach, while

based on the classical monopulse concept, is tailored through an iterative nulling framework to offer a balance between high performance and computational efficiency.

Monopulse beamforming techniques have gained widespread adoption in IoT radar systems due to their ability to estimate target angles using a single snapshot of received signals with reasonable computational complexity [25], [26], [27], [28], [29], [30]. However, applying these techniques to scenarios involving multiple closely spaced drones presents considerable challenges. The interference from adjacent targets can severely distort the sum and difference beam outputs, leading to inaccurate monopulse ratios (Here, the monopulse ratio is defined as the difference-to-sum ratio (DSR) of the difference beam output to the sum beam output) and consequently, erroneous angle estimates. This issue is particularly problematic in urban IoT environments where multiple drones may operate in close proximity [31]. In most previous works [26], [27], [28], [30], multiple closely-spaced targets are not considered, assuming that a single target is located within the beamwidth of the sum beam. In [32] and [33], they consider that the radar signal is composed of the direct path signal and the surface-reflected path signal from a single target. The AoAs of two signal components lie within the array antenna beamwidth and the angular separation between the two is small. Here, by exploiting the geometrical relation between the AoAs of direct and specular paths, the estimation of two angles boils down to a single-target angle estimation problem, which is not possible to multiple closely-spaced target angle estimation.

This paper proposes an iterative monopulse beamforming approach that addresses these limitations through: (1) a constrained convex optimization formulation for adaptive beam design with nulling constraints, (2) an iterative algorithm that alternately updates beamformers while incorporating interference suppression, and (3) a low-complexity orthogonal projection method with slope and bias calibration for real-time implementation in IoT devices. The proposed method is specifically designed to meet the requirements of IoT applications, including low computational complexity, energy efficiency, and real-time processing capabilities. We note that our approach considers scenarios without predefined geometrical relationships between target angles. The major contributions of this paper are summarized as follows:

- We propose an iterative convex monopulse beamforming algorithm that adaptively refines beamforming weights with updated null constraints. By employing a full common weight vector for both sum and difference beams, we reduce optimization parameters while maintaining performance. The algorithm iteratively updates monopulse beams through convex programming with dynamically adjusted null constraints.
- Furthermore, to reduce computational complexity, we propose a low-complexity iterative nulling algorithm based on orthogonal projection. Specifically, to avoid the process of solving the optimization problem during the iterations, an iterative nulling method is proposed using orthogonal projection. We also analyze the effect

of the orthogonal projection on DSR slope and offset at the boresight angle and then, propose a calibration method to compensate for these effects.

- We validate the proposed algorithms through the computer simulation. In addition, we implement them using the commercial radar module to evaluate the performance in the laboratory experiment. The effectiveness of these proposed methods in mitigating inter-target interference and enhancing angle estimation accuracy is analyzed, providing valuable insights for high-resolution radar in challenging multi-target environments.

To provide a comprehensive overview of the contributions of this work, Table 1 summarizes and compares the proposed methods with existing angle estimation techniques. The comparison highlights the unique advantages of our approach in terms of multi-target capability, computational complexity, and suitability for IoT applications.

The rest of this paper is organized as follows. In Section II, the system model for MIMO FMCW radar is introduced and the monopulse beamforming based angle estimation process is presented. In Section III, convex optimization problem is formulated with constraints of the nullity of difference beam at the boresight angle, interference suppression, and slope control. The iterative convex monopulse beamforming algorithm is also proposed. In Section IV, low-complexity iterative nulling monopulse beamforming algorithm is proposed. In Section V, we present various simulation results. In addition, we also provide experimental results of the proposed algorithms implemented by using the commercial radar module in Section VI. Finally, Section VII presents the concluding remarks.

## II. SYSTEM MODEL AND MONOPULSE BEAMFORMING BASED ANGLE ESTIMATION

### A. SIGNAL MODEL

We consider a MIMO FMCW radar system equipped with a uniform linear array (ULA) composed of  $2M$  antenna elements in Fig. 1. The system aims to estimate the angles of arrival (AoA) of closely spaced multiple targets by processing the received signal at the radar receiver. Specifically, we focus on the challenging scenario where targets are located within the same range-Doppler bin, meaning they cannot be

separated by round-trip time or velocity information alone. After reflecting from  $K$  multiple targets, the received FMCW baseband signal at the  $n$ -th snapshot can then be expressed as

$$\mathbf{x}[n] = \sum_{k=1}^K \alpha_k \mathbf{a}(u_k) \exp\{j2\pi\beta_c \tau_k T_s n + \phi_k\} + \mathbf{n}[n], \quad (1)$$

where  $\alpha_k$  and  $u_k (\triangleq \sin \theta_k)$  denote the aggregated target reflection coefficient and the AoA of the  $k$ -th target, respectively. Without loss of generality, because  $u_k = \sin \theta_k$  is one-to-one mapping for  $\theta_k \in [-\pi/2, \pi/2]$ , we use  $u_k$  for the AoA for simplifying the notation. In addition,  $\beta_c$  and  $T_s$  are the FMCW chirp rate and the sampling time. The propagation time delay and the phase offset are denoted as  $\tau_k$  and  $\phi_k$ , respectively. The time delay can be given as  $2R_k/c$  with  $c = 3 \times 10^8 \text{ m/s}$  and the distance between the radar and the  $k$ -th target. The additive white Gaussian noise is denoted as  $\mathbf{n}[n]$ . The steering vector  $\mathbf{a}(u_k)$  is given by

$$\mathbf{a}(u_k) = \left[ e^{j(M-\frac{1}{2})\frac{2\pi}{\lambda} du_k}, \dots, e^{j\frac{1}{2}\frac{2\pi}{\lambda} du_k}, e^{-j\frac{1}{2}\frac{2\pi}{\lambda} du_k}, \dots, e^{-j(M-\frac{1}{2})\frac{2\pi}{\lambda} du_k} \right]^T, \quad (2)$$

where  $\lambda$  is the wavelength and  $d$  is the inter-element spacing, typically set to  $\lambda/2$ .

### B. MONOPULSE BEAMFORMING BASED ANGLE ESTIMATION PROCESS

In conventional monopulse beamforming, assuming that there is a single target (i.e.,  $K = 1$ ), sum and difference beams are simultaneously formed to estimate the target angle. The monopulse ratio, defined as the ratio of the difference beam output to the sum beam output, provides a slope around the boresight angle that allows for linear angle estimation [33]:

$$\text{DSR} = \Re \left[ \frac{y_{\Delta}(\mathbf{w}_{\Delta,1})}{y_{\Sigma}(\mathbf{w}_{\Sigma,1})} \right], \quad (3)$$

where  $y_{\Sigma}(\mathbf{w}_{\Sigma,1})$  and  $y_{\Delta}(\mathbf{w}_{\Delta,1})$  are the beamformer outputs with the sum and difference beamforming weights ( $\mathbf{w}_{\Sigma,1}$  and  $\mathbf{w}_{\Delta,1}$ ), respectively. That is, the beamformer outputs are computed as

$$y_{\Sigma}(\mathbf{w}_{\Sigma,1}) = \mathbf{w}_{\Sigma,1}^H \mathbf{x}[n], \quad y_{\Delta}(\mathbf{w}_{\Delta,1}) = \mathbf{w}_{\Delta,1}^H \mathbf{x}[n]. \quad (4)$$

Here,  $\Re[\cdot]$  and  $\Im[\cdot]$  denote the real and imaginary parts, respectively. In Fig. 2 (a), the beam patterns are exhibited when Taylor and Bayliss weights are employed for the sum and difference beams with the boresight angle,  $u_b = 0$ . In Fig. 2 (b), the DSR is evaluated around  $u_b$ . If the slope of DSR is given by  $\kappa$ , the target angle can be estimated as:

$$\hat{u}_1 = \frac{1}{\kappa} \Re \left[ \frac{y_{\Delta}(\mathbf{w}_{\Delta,1})}{y_{\Sigma}(\mathbf{w}_{\Sigma,1})} \right] + u_b. \quad (5)$$

In Fig. 1, the monopulse beamforming based angle estimation process is described. In the first step, targets are detected through sequential scanning using sum beams with different boresight angles. Then, the angle of each target can be finely estimated by transmitting the difference beam. When multiple targets are separated by an angle difference

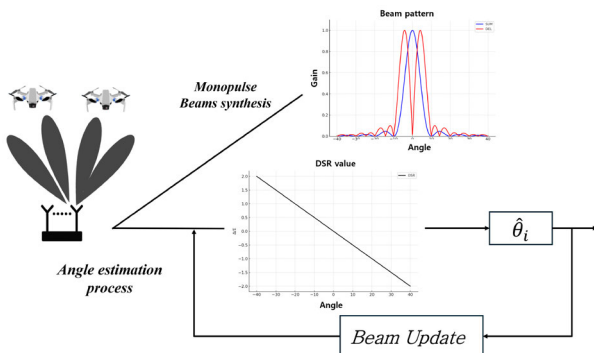


FIGURE 1. Monopulse beamforming based angle estimation system.

TABLE 1. Comparison of angle estimation methods for IoT-enabled multi-target detection.

Method	Multi-target capability	Single snapshot	Real-time processing	Convex optimization	Interference suppression	IoT suitable	Iterative refinement	Calibration method
MUSIC [9], [11], [12]	✓	✗	✗	✗	✗	✗	✗	✗
Conventional Monopulse [25]	✗	✓	✓	✗	✗	✓	✗	✗
Taylor/Bayliss Weights [26]	✗	✓	✓	✗	✗	✓	✗	✗
Compressed Sensing (OMP) [18], [19]	✓	✗	✗	✗	✗	✗	✗	✗
Maximum Likelihood [17]	✓	✗	✗	✗	✗	✗	✗	✗
Adaptive Beamforming [6], [34]	Limited	✓	✓	✓	✓	Limited	✗	✗
<b>Proposed Algorithm 1 (Iterative Convex)</b>	✓	✓	✓	✓	✓	✓	✓	✗
<b>Proposed Algorithm 2 (Low-complexity)</b>	✓	✓	✓	✗	✓	✓	✓	✓

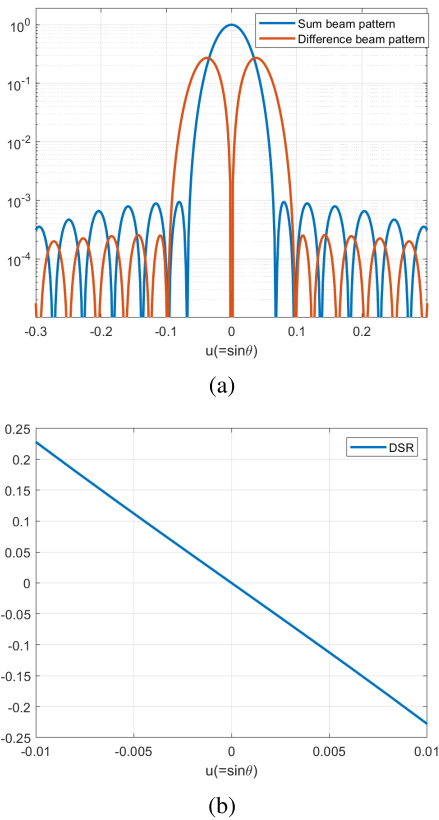


FIGURE 2. (a) Sum and difference beam patterns and (b) DSR when Taylor and Bayliss weights are exploited.

larger than the beam width, and by designing the sum and difference beam patterns to have a low side-lobe level, the target angles are separately estimated using (5). However, when targets are closely spaced, the performance degrades as interference from adjacent signals leads to erroneous angle estimation.

### III. ITERATIVE MULTIPLE TARGET ANGLE ESTIMATION

#### A. CONVEX OPTIMIZATION PROBLEM FOR MONOPULSE BEAM DESIGN

To reduce the number of parameters to be optimized, we consider a full common weight vector to generate sum and difference beams in [26] and [27]. Specifically, the array gains of the sum and difference beam patterns used to

estimate the  $i$ -th target angle are given by:

$$F_{\Sigma,i}(u) = \mathbf{a}^H(u)\mathbf{w}_i, \quad F_{\Delta,i}(u) = \mathbf{a}^H(u)\mathbf{P}_1\mathbf{w}_i, \quad (6)$$

where  $\mathbf{w}_i = [\mathbf{w}_{i,1}^T, \mathbf{w}_{i,2}^T]^T$  with  $\mathbf{w}_{i,1}, \mathbf{w}_{i,2} \in \mathbb{C}^{M \times 1}$ . Here,  $\mathbf{P}_1 = \begin{bmatrix} \mathbf{I}_M & \mathbf{0} \\ \mathbf{0} & \mathbf{I}_M \end{bmatrix}$  and  $\mathbf{I}_M$  is an  $M \times M$  identity matrix. Then, we consider the beam design objective to maximize the beamforming gain of the sum beam while satisfying constraints such as the nullity of difference beam at the boresight angle, sidelobe suppression, and slope control. The joint optimization problem is formulated as:

$$(P.1) \max_{\mathbf{w}_i} |F_{\Sigma,i}(u_b)|^2 \quad (7)$$

s.t. Constraint set 1:

$$F_{\Delta,i}(u_b) = 0 \quad (8)$$

$$|F_{\Sigma,i}(u_s)| \leq \tau_s^2, \quad \forall u_s \in \Theta_{SL} \quad (9)$$

$$|F_{\Delta,i}(u_s)| \leq \tau_s^2, \quad \forall u_s \in \Theta_{SL} \quad (10)$$

$$\left. \frac{\partial F_{\Delta,i}(u)}{\partial u} \right|_{u=u_b} = \kappa F_{\Sigma,i}(u_b) \quad (11)$$

Constraint set 2:

$$F_{\Sigma,i}(u_{c_j}) = 0, \quad \forall u_{c_j} \in \Theta_{NULL,i} \quad (12)$$

$$F_{\Delta,i}(u_{c_j}) = 0, \quad \forall u_{c_j} \in \Theta_{NULL,i} \quad (13)$$

where  $\Theta_{SL}$  indicates the angular region excluding the mainlobe (i.e., sidelobe region) and  $\tau_s$  is a threshold for sidelobe suppression. The constraint (11) ensures that the monopulse ratio has a desired slope  $\kappa$  near the boresight, which is critical for accurate linear angle approximation.  $\Theta_{NULL,i}$  contains the estimated target angles close to the  $i$ -th target angle. In multi-target scenarios, signal leakage from nearby targets may significantly bias AoA estimation. To suppress interference from known or estimated target angles, we impose additional nulling constraints on both sum and difference beams, as shown in Constraint Set 2.

We note that maximizing a convex function, as in (7), is not a convex problem. Therefore, by restricting the weight vector to have a conjugate symmetric structure, as done in [26] and [27], it is transformed into a convex problem. Specifically, in (6), we set

$$\mathbf{w}_{i,2} = \mathbf{P}_2\mathbf{w}_{i,1}^*, \quad (14)$$

where  $\mathbf{P}_2$  denotes an  $M \times M$  anti-diagonal identity matrix, which has 1's on its anti-diagonal positions and 0's elsewhere. Then,  $F_{\Sigma,i}(u)$  can be given as:

$$F_{\Sigma,i}(u) = \Re\{\mathbf{a}^H(u)\mathbf{w}_i\} = \mathbf{a}_S^T(u)\bar{\mathbf{w}}_i, \quad (15)$$

where  $\mathbf{a}_S(u) = \begin{bmatrix} \Re\{\mathbf{a}(u)\}_{1:M} + \mathbf{P}_2\mathbf{a}(u)\}_{M+1:2M} \\ \Im\{\mathbf{a}(u)\}_{1:M} + \mathbf{P}_2\mathbf{a}(u)\}_{M+1:2M} \end{bmatrix}$  and  $\bar{\mathbf{w}}_i = \begin{bmatrix} \Re\{\mathbf{w}_i\} \\ \Im\{\mathbf{w}_i\} \end{bmatrix}$ . Similarly,  $F_{\Delta,i}(u)$  can be given as:

$$F_{\Delta,i}(u) = \Im\{\mathbf{a}^H(u)\mathbf{w}_i\} = \mathbf{a}_D^T(u)\bar{\mathbf{w}}_i, \quad (16)$$

where  $\mathbf{a}_D(u) = \begin{bmatrix} \Re\{\mathbf{a}(u)\}_{1:M} + \mathbf{P}_2\mathbf{a}(u)\}_{M+1:2M} \\ \Im\{\mathbf{a}(u)\}_{1:M} + \mathbf{P}_2\mathbf{a}(u)\}_{M+1:2M} \end{bmatrix}$ . Then, the optimization problem in (7) can be transformed into the convex problem as:

$$(P.2) \max_{\bar{\mathbf{w}}_i} \mathbf{a}_S^T(u_b)\bar{\mathbf{w}}_i \quad (17)$$

s.t. Constraint set 1:

$$\mathbf{a}_D^T(u_b)\bar{\mathbf{w}}_i = 0 \quad (18)$$

$$-\tau_s \leq \mathbf{a}_S^T(u_s)\bar{\mathbf{w}}_i \leq \tau_s, \quad \forall u_s \in \Theta_{SL} \quad (19)$$

$$-\tau_s \leq \mathbf{a}_D^T(u_s)\bar{\mathbf{w}}_i \leq \tau_s, \quad \forall u_s \in \Theta_{SL} \quad (20)$$

$$\left. \frac{\partial \mathbf{a}_D^T(u)}{\partial u} \right|_{u=u_b} \bar{\mathbf{w}}_i = \kappa \mathbf{a}_S^T(u_b)\bar{\mathbf{w}}_i \quad (21)$$

Constraint set 2:

$$\mathbf{a}_S^T(u_{c_j})\bar{\mathbf{w}}_i = 0, \quad \forall u_{c_j} \in \Theta_{NULL,i} \quad (22)$$

$$\mathbf{a}_D^T(u_{c_j})\bar{\mathbf{w}}_i = 0, \quad \forall u_{c_j} \in \Theta_{NULL,i} \quad (23)$$

Because the objective function and the constraints in (P.2) are linear functions of  $\bar{\mathbf{w}}_i$ , it can be effectively solved using convex programming. Once  $\bar{\mathbf{w}}_i$  is obtained,  $\mathbf{w}_i$  can be obtained as

$$\mathbf{w}_i = \begin{bmatrix} [\bar{\mathbf{w}}_i]_{1:M} + j[\bar{\mathbf{w}}_i]_{M+1:2M} \\ \mathbf{P}_2([\bar{\mathbf{w}}_i]_{1:M} - j[\bar{\mathbf{w}}_i]_{M+1:2M}) \end{bmatrix}. \quad (24)$$

We note that the optimization problem in (P.1) is non-convex due to the magnitude square operation in the objective function. However, by imposing a conjugate symmetric structure on the weight vector, we can reformulate it as the equivalent convex problem (P.2). This conjugate symmetric constraint forces the beam pattern to be real-valued, allowing us to replace the magnitude square maximization with linear maximization. Importantly, this transformation preserves the optimal solution - problems (P.1) and (P.2) are mathematically equivalent and yield identical beamformers.

### B. ITERATIVE MULTIPLE TARGET ANGLE ESTIMATION PROCESS

The optimization problem (P.2) in (17) requires the angle information of closely spaced targets. That is, Constraint set 2 forces deep nulls in the undesired directions, thereby reducing the interference on the DSR and improving estimation accuracy for  $\theta_i$ . Accordingly, we propose an iterative convex monopulse beamforming algorithm that adaptively refines the beamforming weights with the updated null constraints. The detailed process is summarized in Algorithm 1.

### Algorithm 1 Iterative Convex Monopulse Beamforming

- 1: **Output:** Estimated angle  $\hat{u}_i, i = 1, \dots, K$ .
- 2: Obtain the common monopulse beamforming weights,  $\mathbf{w}_i$ , from (P.2) with Constraint set 1.
- 3: Estimate initial target angles as
 
$$\hat{u}_i = \frac{1}{\kappa} \frac{y_{\Delta}(\mathbf{w}_i)}{y_{\Sigma}(\mathbf{w}_i)} + u_{b,i}. \quad (25)$$
- 4: Set  $\Theta_{NULL,i}$  for  $i = 1, \dots, K$  based on the estimated target angles.
- 5: Estimate  $\hat{\theta}_2^{(0)}$  using current beam.
- 6: **for**  $n = 1$  to  $N_{iter}$  **do**
- 7:     Obtain  $\mathbf{w}_i$  from (P.2) with Constraint set 1 and 2.
- 8:     Estimate  $\hat{u}_i$  with the updated  $\mathbf{w}_i$  as in (25).
- 9:     Update  $\Theta_{NULL,i}$  for  $i = 1, \dots, K$ .
- 10: **end for**
- 11: **return**  $\hat{u}_i$  for  $i = 1, \dots, K$ .

The key idea is that we do not need to know the interference angles a priori. Instead, we use the estimated angles from the previous iteration to form the nulling constraints for the current iteration. For estimating the angle of the  $i$ -th target, the estimated angles of all other targets,  $\{\hat{u}_j\}_{j \neq i}$ , from the previous step are considered as interference and are included in the null set  $\Theta_{NULL,i}$ .

### IV. LOW-COMPLEXITY ITERATIVE NULLING MONOPULSE BEAMFORMING ALGORITHM

We note that Algorithm 1 requires solving the optimization problem (P.2) at each iteration with updated  $\hat{u}_i$ . To avoid the process of solving the optimization problem, an iterative nulling method is proposed using orthogonal projection. That is, instead of solving the optimization problem (P.2), we project the monopulse beamforming weights onto the orthogonal space with respect to the column space of  $[\mathbf{a}(u_{c1}^{(i)}), \dots, \mathbf{a}(u_{cK_c}^{(i)})]$ . Here,  $u_{c_j}^{(i)} \in \Theta_{NULL,i}$  and  $K_c$  is the number of targets close to the  $i$ -th target. To get insight into the iterative nulling method, let us assume that  $K_c = 1$ . Then, the orthogonal projection with respect to  $\mathbf{a}(u_{c1}^{(i)})$  is given as

$$\begin{aligned} \mathbf{P}_i^\perp &= \mathbf{I}_{2M} - \mathbf{a}(u_{c1}^{(i)})\mathbf{a}(u_{c1}^{(i)})^H\mathbf{a}(u_{c1}^{(i)})^{-1}\mathbf{a}^H(u_{c1}^{(i)}) \\ &= \mathbf{I}_{2M} - \frac{1}{2M}\mathbf{a}(u_{c1}^{(i)})\mathbf{a}^H(u_{c1}^{(i)}). \end{aligned} \quad (26)$$

From (6), the projected sum and difference beam weights are given as

$$\mathbf{w}_{\Sigma,i} = \mathbf{w}_i - \frac{\mathbf{a}^H(u_{c1}^{(i)})\mathbf{w}_i}{2M}\mathbf{a}(u_{c1}^{(i)}), \quad (27)$$

$$\mathbf{w}_{\Delta,i} = \mathbf{P}_1\mathbf{w}_i - \frac{\mathbf{a}^H(u_{c1}^{(i)})\mathbf{P}_1\mathbf{w}_i}{2M}\mathbf{a}(u_{c1}^{(i)}). \quad (28)$$

The updated  $\mathbf{w}_{\Sigma,i}$  and  $\mathbf{w}_{\Delta,i}$  suppress the interference from the direction of  $u_{c1}^{(i)}$ , but the optimization constraints in (P.2) are not satisfied. That is, the DSR slope is no longer  $\kappa$ , and the DSR is biased at  $u_b$ . Specifically, when  $\mathbf{w}_{\Sigma,i}$  and  $\mathbf{w}_{\Delta,i}$

are utilized, from (6) and (11), the DSR around  $u_b$  can be approximated as

$$\begin{aligned} \kappa_n &= \frac{1}{\mathbf{a}^H(u_b)\mathbf{w}_{\Sigma,i}} \left. \frac{\partial \mathbf{a}^H(u)\mathbf{w}_{\Delta,i}}{\partial u} \right|_{u=u_b} \\ &= \frac{1}{\mathbf{a}^H(u_b)\mathbf{w}_i - \Delta S} \left( \left. \frac{\partial \mathbf{a}^H(u)\mathbf{P}_1\mathbf{w}_i}{\partial u} \right|_{u=u_b} - \Delta D \right), \end{aligned} \quad (29)$$

where

$$\Delta S = \frac{\mathbf{a}^H(u_{c1}^{(i)})\mathbf{w}_i\mathbf{a}^H(u_b)\mathbf{a}(u_{c1}^{(i)})}{2M}, \quad (30)$$

$$\Delta D = \frac{\mathbf{a}^H(u_{c1}^{(i)})\mathbf{P}_1\mathbf{w}_i \left. \frac{\partial \mathbf{a}^H(u)}{\partial u} \right|_{u=u_b} \mathbf{a}(u_{c1}^{(i)})}{2M}. \quad (31)$$

Then, for small  $\Delta S$  and  $\Delta D$ ,  $\kappa_n$  can be approximated as

$$\kappa_n = \kappa + \kappa \left( \frac{\Delta S}{\mathbf{a}^H(u_b)\mathbf{w}_i} - \frac{\Delta D}{\left. \frac{\partial \mathbf{a}^H(u)\mathbf{P}_1\mathbf{w}_i}{\partial u} \right|_{u=u_b}} \right). \quad (32)$$

The bias at  $u_b$  is given as

$$\beta_n = -\frac{\mathbf{a}^H(u_{c1}^{(i)})\mathbf{P}_1\mathbf{w}_i\mathbf{a}^H(u_b)\mathbf{a}(u_{c1}^{(i)})}{2M(\mathbf{a}^H(u_b)\mathbf{w}_i - \Delta S)}. \quad (33)$$

Therefore, the target angle can be estimated as:

$$\hat{u}_i = \frac{1}{\kappa_n} \left( \frac{y_{\Delta}(\mathbf{w}_{\Delta,i})}{y_{\Sigma}(\mathbf{w}_{\Sigma,i})} - \beta_n \right) + u_{b,i}. \quad (34)$$

In Algorithm 2, iterative nulling monopulse beamforming algorithm with slope and bias calibration is summarized.

**Algorithm 2** Iterative Nulling Monopulse Beamforming With Slope and Bias Calibration

- 1: **Output:** Estimated angle  $\hat{u}_i, i = 1, \dots, K$ .
- 2: Obtain the common monopulse beamforming weights,  $\mathbf{w}_i$ , from (P.2) with Constraint set 1.
- 3: Estimate initial target angles as

$$\hat{u}_i = \frac{1}{\kappa} \frac{y_{\Delta}(\mathbf{w}_i)}{y_{\Sigma}(\mathbf{w}_i)} + u_{b,i}. \quad (35)$$

- 4: Set  $\Theta_{\text{NULL},i}$  for  $i = 1, \dots, K$  based on the estimated target angles.
- 5: **for**  $n = 1$  to  $N_{\text{iter}}$  **do**
- 6:     Obtain  $\mathbf{w}_{\Sigma,i}$  and  $\mathbf{w}_{\Delta,i}$  from (27) and (28).
- 7:     Update DSR slope and bias at  $u_b$  as (32) and (33).
- 8:     Estimate  $\hat{u}_i$  using (34).
- 9:     Update  $\Theta_{\text{NULL},i}$  for  $i = 1, \dots, K$ .
- 10: **end for**
- 11: **return**  $\hat{u}_i$  for  $i = 1, \dots, K$ .

In Figs. 3 (a) and 3 (b), sum and difference beam patterns are exhibited when Algorithm 1 and Algorithm 2 are exploited with  $M = 22$ , respectively. Here, the boresight angle is given as  $u_b = 0$ , and the interfering target is located at  $u_{c1} = \sin(5/180\pi) = 0.087$ . From Figs. 3 (a) and 3 (b), both sum and difference beam patterns show a null

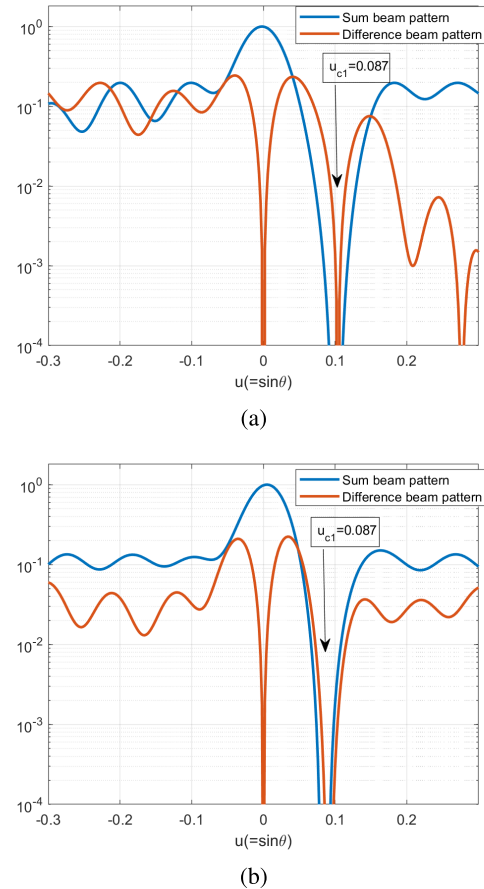


**FIGURE 3.** Sum and difference beam patterns when (a) Algorithm 1 and (b) Algorithm 2 are exploited. Here, the interfering target is located at  $u_{c1} = \sin(5/180\pi) = 0.087$ .

at  $u_{c1} = \sin(5/180\pi) = 0.087$ , regardless of the algorithm used. We note that the optimized beamforming weights can be achieved using Algorithm 2, efficiently avoiding the iterative optimization problem-solving process. In Fig. 4, DSR values are evaluated when Algorithm 1 and Algorithm 2 are exploited, respectively. It can be observed that, due to the orthogonal projection, the slope of the DSR with Algorithm 2 is changed and a non-zero offset is observed at  $u_b = 0$ . Therefore, when orthogonally projected monopulse beamforming weights are utilized, the target angles need to be estimated using the calibrated slope and the non-zero offset, as shown in (34).

*Remark 1:* (Computational complexity analysis) When the interior point method is used, the computational complexity of solving the convex problem in (P.2) is  $O((N_c)^{3/2}(2M)^2)$ , where  $N_c$  is the number of linear constraints. For example, if  $\Theta_{\text{SL}}$  has  $N_s$  sample points,  $N_c$  is approximately  $2N_s$  [35]. Therefore, the computational complexity of Algorithm 1 is  $O(N_{\text{iter}}(2N_s)^{3/2}(2M)^2)$ , where  $N_{\text{iter}}$  is the iteration number of Algorithm 1. In contrast, Algorithm 2 requires only one convex problem-solving process at the beginning and four inner products of  $2M \times 1$  vectors at each iteration. Therefore, the computational

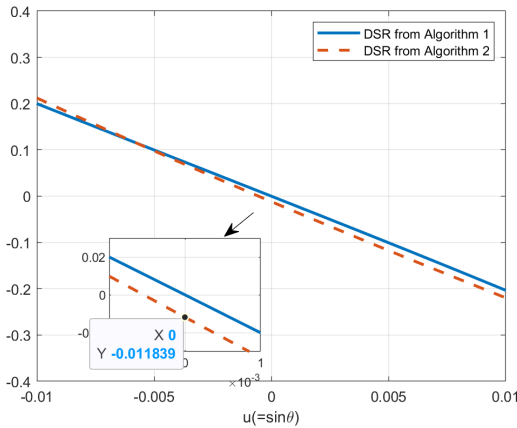


FIGURE 4. DSRs when Algorithm 1 and Algorithm 2 are exploited.

complexity of Algorithm 2 is  $O((2N_s)^{3/2}(2M)^2 + 8N_{iter}M)$ . To provide a more concrete comparison, let us consider specific parameter values ( $M = 20$ ,  $N_s = 180$  (sidelobe constraint points), and  $N_{iter} = 5$  iterations). Under these conditions:

- Algorithm 1:  $O(5 \times 360^{1.5} \times 1600) \approx O(5.5 \times 10^7)$
- Algorithm 2:  $O(360^{1.5} \times 1600 + 8 \times 5 \times 20) \approx O(1.1 \times 10^7)$

This shows Algorithm 2 achieves approximately  $5 \times$  computational savings. The key advantage of Algorithm 2 is that it solves the convex optimization problem only once at initialization, then uses simple vector operations (inner products) for subsequent iterations, making it much more suitable for real-time implementation. We also note that, while MUSIC does not require beam updates, it has its own significant computational burdens that make it challenging for real-time IoT applications: 1) Eigenvalue Decomposition: MUSIC requires computing the eigenvalue decomposition of the  $(2M \times 2M)$  covariance matrix, which has complexity  $O((2M)^3) = O(8M^3)$ . 2) Spectrum evaluation: MUSIC requires evaluating the pseudo-spectrum over a dense angular grid (typically hundreds of points) to locate peaks, with complexity  $O(N_{grid} \times (2M)^2)$  where  $N_{grid}$  is the number of search points. 3) Spectral Search and peak detection: Reliable peak detection in the presence of noise requires sophisticated algorithms and multiple snapshots for averaging. In contrast, our Algorithm 2 performs the convex optimization only once at initialization and then uses simple vector operations ( $O(M)$  per iteration). This makes our approach more suitable for resource-constrained IoT devices requiring real-time processing.

## V. SIMULATION RESULTS

This section presents a comprehensive performance evaluation of the proposed iterative convex monopulse beamforming techniques for multiple target scenarios through extensive computer simulations.

### A. SIMULATION SETUP

We consider a uniform linear array with  $2M = 40$  antenna elements spaced by  $d = \lambda/2$  and operating at a carrier

frequency of 24 GHz. Two targets are placed within the field of view and Table 2 summarizes the key simulation parameters. These parameters are from a typical automotive radar specification in [36], [37], but they can be extended to other parameters on common commercial radar modules, as given in Table 4. The rationale for key constraints involves a deliberate trade-off: the sidelobe threshold ( $\tau_s = 0.2$ ) is selected to maintain robust general interference suppression while preserving sufficient degrees of freedom for the adaptive nulling algorithms (Algorithms 1 and 2). Similarly, the DSR slope ( $\kappa = -26$ ) is chosen to ensure a steep and linear response in the boresight region, which is critical for estimation accuracy.

TABLE 2. Simulation parameters.

Parameter	Value
Number of antennas ( $2M$ )	40
Carrier frequency $f_c$	24 GHz
Wavelength $\lambda$	12.5 mm
Inter-element spacing $d$	$\lambda/2$
Angle for target 1	$[-1.5^\circ, 1.5^\circ]$
Angle for target 2	$[2.5^\circ, 3.5^\circ]$ $[4.5^\circ, 5.5^\circ]$
Boresight angles	$0^\circ$ for Target 1 $5^\circ$ for Target 2
Sidelobe threshold ( $\tau_s$ )	0.2
DSR slope constraint ( $\kappa$ )	-26
Number of samples in $\Theta_{SL}$ ( $N_s$ )	914

### B. CONVERGENCE ANALYSIS OF PROPOSED ALGORITHMS

Fig. 5 shows how the AoA estimate of two targets ( $\hat{u}_1$  and  $\hat{u}_2$ ) converges over successive iterations when using the proposed iterative nulling methods (i.e., Algorithm 1 and Algorithm 2). The initial estimates exhibit bias due to mutual interference between targets. However, as the iterations proceed, the estimated angle converges rapidly toward the true target angle. This demonstrates the effectiveness of the proposed method to dynamically suppress mutual interference and accurately localize the targets even under closely spaced multi-source conditions.

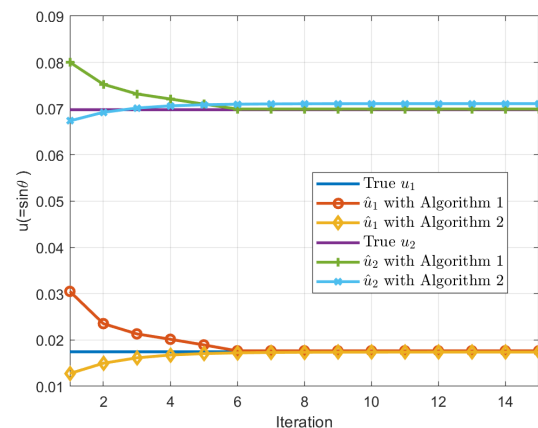


FIGURE 5. Convergence of estimated angles  $\hat{\theta}_1$  and  $\hat{\theta}_2$  with iterative nulling methods. (Algorithm 1 and Algorithm 2).

C. MSE PERFORMANCE ANALYSIS

Fig. 6 presents the MSE of the estimated angle  $\hat{\theta}_1$  across a range of SNR values from -10 to 20 dB. We compare the performance of our proposed iterative convex monopulse beamforming (Algorithm 1) and iterative nulling monopulse beamforming (Algorithm 2) with non-iterative convex monopulse beamforming. In addition, the MSEs of the MUSIC algorithm [9], [11] and Orthogonal Matching Pursuit (OMP) [18] are also evaluated. To provide a fundamental benchmark for evaluating AoA estimation performance, CRB is also evaluated. For our signal model in (1), following the classical derivation in [38] and [39], the CRB for the  $k$ -th target angle is given by:

$$CRB(\theta_k) = \frac{\sigma_n^2}{2N_{sn} \cdot E[|\alpha_k|^2]} [\mathbf{D}_k^H \mathbf{P}_{\mathbf{A}_k}^\perp \mathbf{D}_k]^{-1} \quad (36)$$

where  $N_{sn}$  is the number of snapshots,  $\mathbf{D}_k = \frac{\partial \mathbf{a}(\theta_k)}{\partial \theta_k}$  is the derivative of the steering vector, and  $\mathbf{P}_{\mathbf{A}_k}^\perp = \mathbf{I} - \mathbf{A}_k(\mathbf{A}_k^H \mathbf{A}_k)^{-1} \mathbf{A}_k^H$  is the projection matrix orthogonal to the interference subspace. Here,  $\mathbf{A}_k$  contains the steering vectors of all targets except the  $k$ -th target.

The results demonstrate that the proposed iterative convex monopulse beamforming consistently outperforms other methods, primarily due to its adaptive optimization of monopulse beam patterns through updated interference nulling constraints at each iteration. The iterative nulling monopulse beamforming (Algorithm 2) also shows superior performance compared to conventional non-iterative methods, which is comparable to MUSIC algorithm with 100 snapshots. We note that Algorithm 2 avoids the computational burden of solving optimization problems in each iteration. At low SNR levels, the interference nulling constraints do not significantly improve the MSE performance of Algorithms 1 and 2 due to the inherent difficulty in accurately estimating target angles. However, at higher SNR levels, the proposed framework effectively handles strong interference and significantly improves localization accuracy. We also note that in Fig. 6(a), the MSE curves for the proposed methods exhibit an error floor at high SNR levels. This floor is caused by residual inter-target interference, which becomes the dominant error source when thermal noise is negligible. The fundamental cause of this residual interference is the high spatial correlation between steering vectors when targets are very closely spaced. This is empirically confirmed by comparing Fig. 6(a) and Fig. 6(b): when the targets are placed farther apart (Fig. 6(b)), the interference is weaker, and the MSE floor for Algorithm 1 disappears entirely within the observed SNR range. Quantitatively, in Fig. 6(b), to achieve an MSE of  $10^{-5}$ , the proposed Algorithm 1 requires approximately 5 dB SNR, whereas the conventional monopulse method fails to reach this accuracy even at 20 dB SNR, demonstrating a significant SNR gain of more than 15 dB.

In Fig. 7, we have conducted a simulation to evaluate the bias of the AoA estimates. That is,  $E[\hat{u}_i - u_i]$  is evaluated for two proposed beamforming methods. The

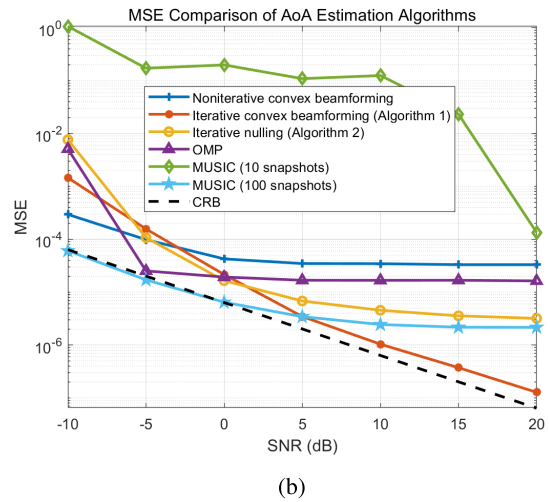
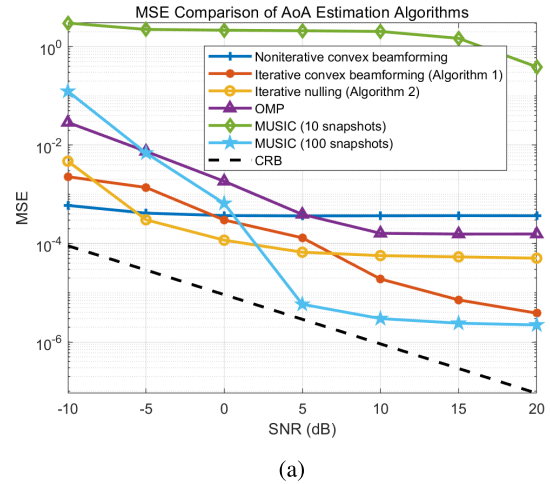


FIGURE 6. MSE versus SNR for various beamforming methods when (a)  $\theta_2 \in [2.5^\circ, 3.5^\circ]$  (b)  $\theta_2 \in [4.5^\circ, 5.5^\circ]$  with  $\theta_1 \in [-1.5^\circ, 1.5^\circ]$ .

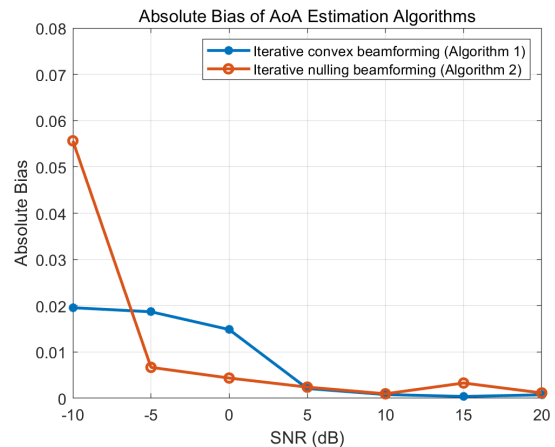


FIGURE 7. Bias versus SNR for the proposed beamforming methods.

results clearly show that the bias of our proposed iterative methods approaches to zero as SNR goes high.

In Fig. 8, the angular resolution capability of the proposed methods is evaluated. Specifically, MSE performance is

evaluated for various angle separation ( $\Delta$ ) when  $\theta_1 \in [-1.5, 1.5]$  and  $\theta_2 \in [1.5, 2.5] + \Delta$ . Here, we focus on the small angular separation range ( $\Delta \in [0.5^\circ, 1.5^\circ]$ ) specifically to investigate the super-resolution capability in the challenging region below the Rayleigh limit. The results show that as the angular separation decreases, the MSE of conventional methods degrades rapidly. In contrast, the proposed schemes (Algorithm 1 and 2) effectively suppress inter-target interference and maintain a low MSE, empirically demonstrating their super-resolution capability to resolve targets spaced closer than the array's conventional Rayleigh limit (i.e.,  $\frac{\lambda}{2Md} \times \frac{180}{\pi} \approx 2.86^\circ$  for our array with  $2M = 40$ ).

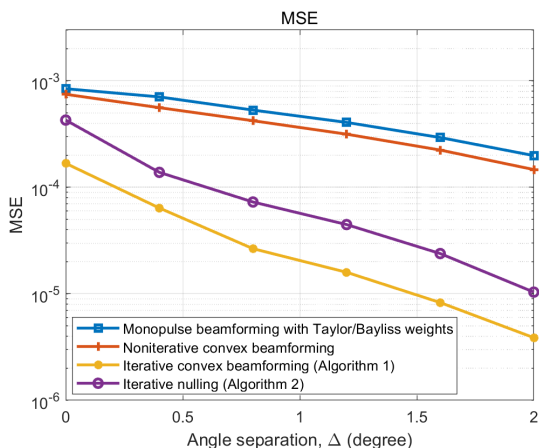
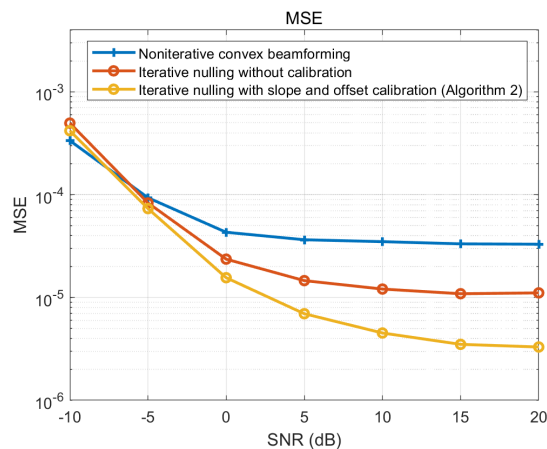


FIGURE 8. MSE versus Angle separation for various monopulse beamforming methods.

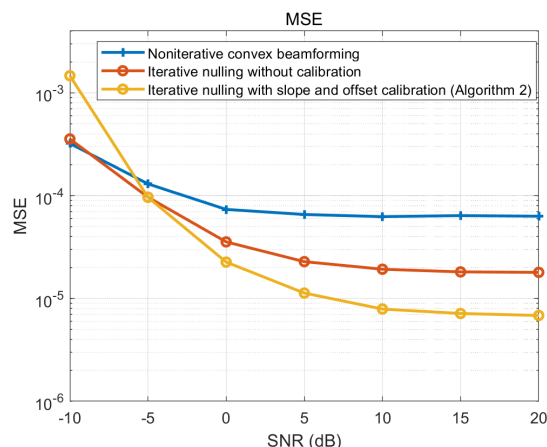
D. IMPACT OF SLOPE AND BIAS CALIBRATION

To demonstrate the effectiveness of the slope and bias calibration in Algorithm 2, Fig. 9 compares the MSE performance of the iterative nulling monopulse beamforming with and without calibration for (a) two targets and (b) three targets. The results clearly show that the uncalibrated version exhibits significantly worse performance, highlighting the importance of compensating for the changes in DSR slope and non-zero offset at  $u_b$  caused by orthogonal projection. The proposed calibration method effectively mitigates these effects, leading to improved estimation accuracy. Furthermore, Fig. 9(b) validates the scalability of the proposed method by demonstrating its effectiveness in a three-target scenario. Although the overall MSE is higher than the two-target case, the iterative nulling process successfully suppresses the complex multi-target interference, achieving a low MSE at high SNR and confirming the method's capability to resolve more than two targets.

To provide a quantitative validation of the computational load, Table 3 shows the measured runtime per frame for each algorithm, executed on a standard Intel Core i9 CPU with  $2M = 40$  and  $N_{iter} = 5$ . For comparison, the computing times for the MUSIC and OMP benchmarks are also evaluated. The results confirm that Algorithm 1 is the most computationally intensive (3.76 s), as it requires solving



(a)



(b)

FIGURE 9. MSE versus SNR for iterative nulling monopulse beamforming with and without the calibration for (a) two targets and (b) three targets.

TABLE 3. Computing time for angle estimation process.

Algorithm	Computing time per frame
MUSIC (100 snapshots)	31.9 ms
OMP	4.1 ms
Iterative convex beamforming (Algorithm 1)	3.76 s
Iterative nulling (Algorithm 2)	0.39 ms

the convex optimization problem at each iteration. In contrast, Algorithm 2 is exceptionally efficient (0.39 ms). It is not only orders of magnitude faster than Algorithm 1 but also significantly outperforms the high-resolution benchmarks, running approximately 10 times faster than OMP and 80 times faster than MUSIC (100 snapshots). This result, combined with its comparable MSE performance (shown in Fig. 6), validates the practical feasibility of Algorithm 2 for real-time, resource-constrained IoT applications.

VI. EXPERIMENTAL RESULTS

This section presents experimental validation of the proposed algorithm's performance in a laboratory environment. We demonstrate that the iterative nulling monopulse

beamforming can achieve real-time accurate angle estimation even in practical, noisy environments.

**A. EXPERIMENTAL SETUP**

Fig. 10 (a) illustrates the experimental setup, which consists of an off-the-shelf FMCW MIMO radar module, a control PC, and two UAVs serving as targets. In Fig. 10 (b), FMCW radar frame structure is given, where each frame consists of 384 chirps and the frame duration is given 125.34ms. We employ the TI AWR2944 FMCW MIMO radar module, with system specifications detailed in Table 4. Here, although the physical antenna count is small, the MIMO configuration ( $N_{Tx} = 3, N_{Rx} = 4$ ) creates a virtual array of 12 elements, providing sufficient aperture for beamforming. While the large bandwidth provides high range resolution, beamforming is indispensable for resolving targets located at the same range.

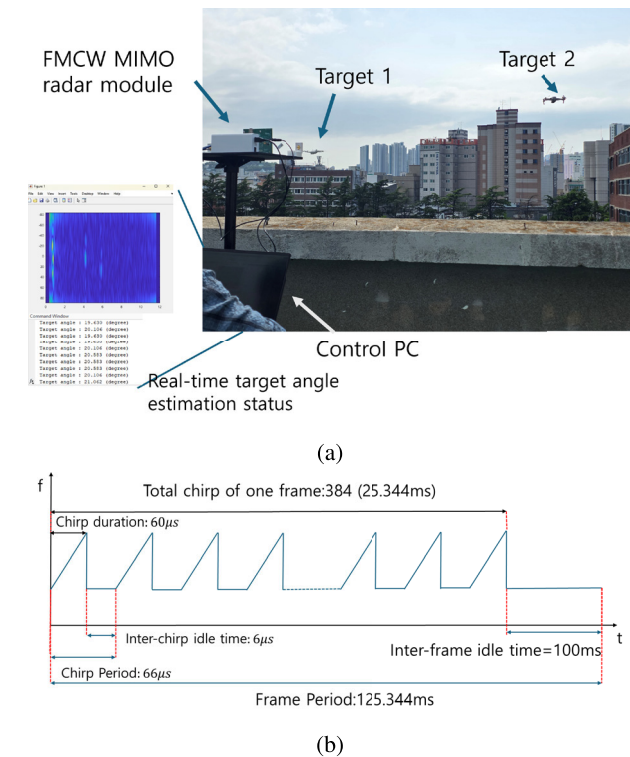


**FIGURE 10. (a) Experimental setup and (b) FMCW radar frame structure.**

The experimental scenario involves two UAVs in urban airspace: one hovering at an azimuth angle of  $-10^\circ$  and another moving laterally. We implement Algorithm 2 to estimate both target angles in real-time, with the estimated angles recorded in the control PC. To validate the practical applicability and substantiate the real-time processing, we analyzed the processing latency within our experimental setup. The processing flow per frame is as follows: the de-ramped data is received, range DFT is applied for target detection, and then ten samples from the detected range bins are used by Algorithm 2 to estimate the AoA. The total time budget available for this entire process is dictated by

the frame duration, which is 125.34 ms as in Fig. 10 (b). As shown in Table 3, the measured execution time for our proposed Algorithm 2 is only 0.39 ms. While this benchmark was obtained on a standard Intel Core i9 CPU, not an IoT device, this extremely low latency provides massive computational headroom. Even if a resource-constrained embedded processor (e.g., NVIDIA Jetson or similar) were 100 times slower, the resulting processing time (approx. 39 ms) would still be comfortably within the 125.34 ms frame budget. This analysis confirms the practical feasibility of Algorithm 2 for real-time IoT applications. For comparison, we have saved the raw radar data to compute the MUSIC spectrum offline using 128 chirp samples, as its high latency (shown in Table 3) is prohibitive for real-time implementation.

**TABLE 4. Experimental parameters for FMCW radar system.**

Parameter	Value
Carrier frequency $f_c$	77 GHz
Wavelength $\lambda$	3.896 mm
Bandwidth $B$	1.798 GHz
Chirp duration	60 $\mu$ s
ADC sampling rate	6000 ksps
TX antennas $N_{Tx}$	3
RX antennas $N_{Rx}$	4
Samples per chirp	256
Chirps per frame	384
Total frames collected	250
Number of targets	2

**B. ANGLE TRACKING PERFORMANCE**

Fig. 11 presents the angle tracking results for both (a) conventional monopulse beamforming and (b) the proposed iterative nulling monopulse beamforming (Algorithm 2). As a baseline reference, the high-resolution MUSIC spectrum is computed offline, revealing the two target tracks. Fig. 11 presents the angle tracking results for both (a) conventional monopulse beamforming and (b) the proposed iterative nulling monopulse beamforming (Algorithm 2). As a baseline reference, the high-resolution MUSIC spectrum is computed offline, revealing the two target tracks. In Fig. 11(a), the conventional method’s angle estimates are clearly corrupted when the targets are closely spaced. In contrast, Fig. 11(b) shows that the proposed iterative nulling method provides significantly improved and more stable angle estimates, effectively mitigating the off-angle interference.

To supplement this qualitative analysis with a quantitative one, we performed an RMSE analysis. Obtaining precise ground truth for the moving UAV is challenging in a live experiment. Therefore, we used the stationary UAV (Target 1) as a robust performance measure. Any deviation in its angle estimate is a direct measurement of the algorithm’s failure to reject interference from the moving UAV (Target 2). We established a pseudo-ground truth reference for the stationary target by time-averaging the offline MUSIC estimates. Against this reference, the conventional monopulse method yielded a very high RMSE of  $9.76^\circ$ , confirming it was severely impacted by the interference. In contrast,

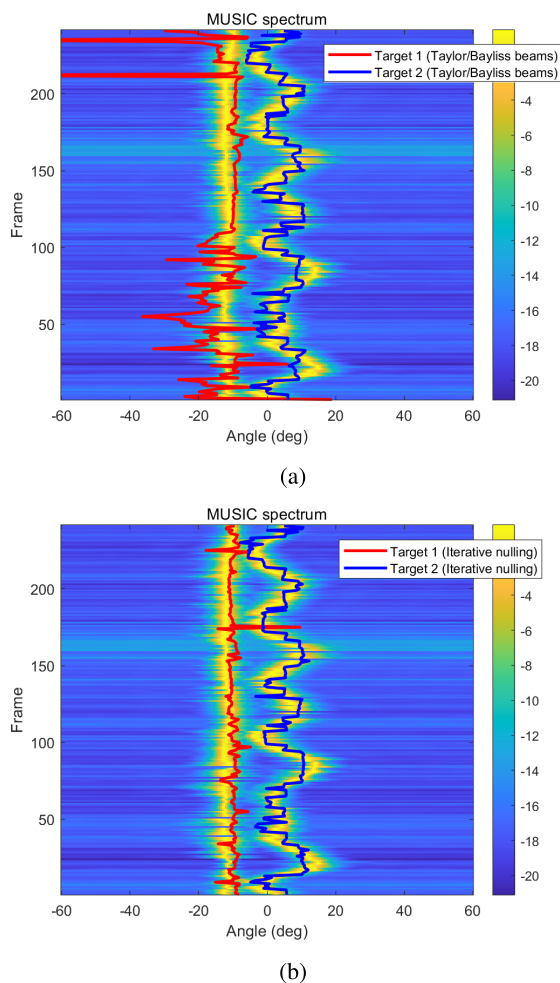


**FIGURE 11.** Angle tracking results when (a) the conventional monopulse beamforming and (b) the proposed iterative nulling monopulse beamforming are exploited.

the proposed iterative nulling monopulse beamforming (Algorithm 2) achieved a low RMSE of  $1.83^\circ$ . This quantitative result powerfully reinforces our claim of superior interference mitigation and tracking accuracy in a real-world context.

While the physical experiment was conducted with two UAVs due to operational and safety constraints, the scalability of the proposed algorithm to scenarios with more than two targets is validated through the comprehensive simulations presented in Section V-D.

## VII. CONCLUSION

This paper presented an iterative monopulse beamforming technique for multi-target angle estimation in IoT-enabled FMCW MIMO radar systems, with a specific focus on drone detection and tracking applications. The convex optimization framework with adaptive nulling constraints effectively suppresses inter-target interference, making it particularly suitable for urban IoT environments where multiple drones may operate simultaneously. The key contributions include: (1) a constrained convex formulation enabling precise beam

control, (2) an iterative algorithm with adaptive nulling, and (3) a low-complexity orthogonal projection method with slope and bias calibration. These contributions are specifically designed to meet the requirements of IoT applications, including low computational complexity and energy efficiency.

Simulation and experimental results demonstrate up to 70% MSE reduction compared to conventional methods, confirming practical applicability for IoT-based drone detection and tracking systems. The proposed method's ability to handle closely spaced targets makes it particularly valuable for urban IoT applications where multiple drones may operate in close proximity. The low-complexity implementation ensures that the method can be deployed on resource-constrained IoT devices, making it suitable for widespread adoption in smart city applications, security systems, and airspace management.

## REFERENCES

- [1] M. Alhafnawi, H. A. Bany Salameh, A. Masadeh, H. Al-Obiedollah, M. Ayyash, R. El-Khazali, and H. Elgala, "A survey of indoor and outdoor UAV-based target tracking systems: Current status, challenges, technologies, and future directions," *IEEE Access*, vol. 11, pp. 68324–68339, 2023.
- [2] R. Karim, A. Iftikhar, B. Ijaz, and I. Ben Mabrouk, "The potentials, challenges, and future directions of on-chip-antennas for emerging wireless applications—A comprehensive survey," *IEEE Access*, vol. 7, pp. 173897–173934, 2019.
- [3] H. Hong, J. Zhao, T. Hong, and T. Tang, "Radar–communication integration for 6G massive IoT services," *IEEE Internet Things J.*, vol. 9, no. 16, pp. 14511–14520, Aug. 2022.
- [4] L. M. S. Bine, A. Boukerche, L. B. Ruiz, and A. A. F. Loureiro, "Connecting Internet of Drones and urban computing: Methods, protocols and applications," *Comput. Netw.*, vol. 239, Feb. 2024, Art. no. 110136.
- [5] Y. Liu, M. Peng, G. Shou, Y. Chen, and S. Chen, "Toward edge intelligence: Multiaccess edge computing for 5G and Internet of Things," *IEEE Internet Things J.*, vol. 7, no. 8, pp. 6722–6747, Aug. 2020.
- [6] J. Li and P. Stoica, "MIMO radar with colocated antennas," *IEEE Signal Process. Mag.*, vol. 24, no. 5, pp. 106–114, Sep. 2007.
- [7] C. Duofang, C. Baixiao, and Q. Guodong, "Angle estimation using ESPRIT in MIMO radar," *Electron. Lett.*, vol. 44, no. 12, pp. 770–771, Jun. 2008.
- [8] G. H. Jajamovich, M. Lops, and X. Wang, "Space-time coding for MIMO radar detection and ranging," *IEEE Trans. Signal Process.*, vol. 58, no. 12, pp. 6195–6206, Dec. 2010.
- [9] P. Stoica and A. Nehorai, "MUSIC, maximum likelihood, and Cramer–Rao bound," *IEEE Trans. Acoust., Speech, Signal Process.*, vol. 37, no. 5, pp. 720–741, May 1989.
- [10] C. P. Mathews and M. D. Zoltowski, "Eigenstructure techniques for 2-D angle estimation with uniform circular arrays," *IEEE Trans. Signal Process.*, vol. 42, no. 9, pp. 2395–2407, Sep. 1994.
- [11] R. Schmidt, "Multiple emitter location and signal parameter estimation," *IEEE Trans. Antennas Propag.*, vol. AP-34, no. 3, pp. 276–280, Mar. 1986.
- [12] M. Gunia, A. Zinke, N. Joram, and F. Ellinger, "Analysis and design of a MuSiC-based angle of arrival positioning system," *ACM Trans. Sensor Netw.*, vol. 19, no. 3, pp. 1–41, Mar. 2023, doi: 10.1145/3577927.
- [13] R. Zhang, L. Cheng, S. Wang, Y. Lou, Y. Gao, W. Wu, and D. W. K. Ng, "Integrated sensing and communication with massive MIMO: A unified tensor approach for channel and target parameter estimation," *IEEE Trans. Wireless Commun.*, vol. 23, no. 8, pp. 8571–8587, Aug. 2024.
- [14] R. Zhang, X. Wu, Y. Lou, F.-G. Yan, Z. Zhou, W. Wu, and C. Yuen, "Channel-training-aided target sensing for terahertz integrated sensing and massive MIMO communications," *IEEE Internet Things J.*, vol. 12, no. 4, pp. 3755–3770, Feb. 2025.
- [15] R. Zhang, B. Shim, and W. Wu, "Direction-of-arrival estimation for large antenna arrays with hybrid analog and digital architectures," *IEEE Trans. Signal Process.*, vol. 70, pp. 72–88, 2022.

- [16] Y. Cheng, H. Gu, and W. Su, "Joint 4-D angle and Doppler shift estimation via tensor decomposition for MIMO array," *IEEE Commun. Lett.*, vol. 16, no. 6, pp. 917–920, Jun. 2012.
- [17] S. Kay, *Fundamentals of Statistical Signal Processing: Detection Theory*. Upper Saddle River, NJ, USA: Prentice-Hall, 1998.
- [18] A. Bazzi, D. T. M. Slock, L. Meilhac, and S. Panneerselvan, "A comparative study of sparse recovery and compressed sensing algorithms with application to AoA estimation," in *Proc. IEEE 17th Int. Workshop Signal Process. Adv. Wireless Commun. (SPAWC)*, Jul. 2016, pp. 1–5.
- [19] A. Aich and P. Palanisamy, "On application of OMP and CoSaMP algorithms for DOA estimation problem," in *Proc. Int. Conf. Commun. Signal Process. (ICCCSP)*, Apr. 2017, pp. 1983–1987.
- [20] A. Bazzi, D. T. M. Slock, and L. Meilhac, "Sparse recovery using an iterative variational Bayes algorithm and application to AoA estimation," in *Proc. IEEE Int. Symp. Signal Process. Inf. Technol. (ISSPIT)*, Dec. 2016, pp. 197–202.
- [21] A. Bazzi, D. T. M. Slock, and L. Meilhac, "A Newton-type forward backward greedy method for multi-snapshot compressed sensing," in *Proc. 51st Asilomar Conf. Signals, Syst., Comput.*, Oct. 2017, pp. 1178–1182.
- [22] A. M. Elbir, "DeepMUSIC: Multiple signal classification via deep learning," *IEEE Sensors Lett.*, vol. 4, no. 4, pp. 1–4, Apr. 2020.
- [23] Y. Yuan, S. Wu, M. Wu, and N. Yuan, "Unsupervised learning strategy for direction-of-arrival estimation network," *IEEE Signal Process. Lett.*, vol. 28, pp. 1450–1454, 2021.
- [24] J. Fuchs, M. Gardill, M. Lübke, A. Dubey, and F. Lurz, "A machine learning perspective on automotive radar direction of arrival estimation," *IEEE Access*, vol. 10, pp. 6775–6797, 2022.
- [25] B. R. Mahafza, *Radar Systems Analysis and Design Using MATLAB*. London, U.K.: Chapman & Hall, 2005.
- [26] A. F. Morabito and P. Rocca, "Optimal synthesis of sum and difference patterns with arbitrary sidelobes subject to common excitations constraints," *IEEE Antennas Wireless Propag. Lett.*, vol. 9, pp. 623–626, 2010.
- [27] S. Kwak, J. Chun, D. Park, Y. K. Ko, and B. L. Cho, "Asymmetric sum and difference beam pattern synthesis with a common weight vector," *IEEE Antennas Wireless Propag. Lett.*, vol. 15, pp. 1622–1625, 2016.
- [28] A. F. Morabito and P. Rocca, "Reducing the number of elements in phase-only reconfigurable arrays generating sum and difference patterns," *IEEE Antennas Wireless Propag. Lett.*, vol. 14, pp. 1338–1341, 2015.
- [29] G. Oliveri, M. Carlin, and A. Massa, "Complex-weight sparse linear array synthesis by Bayesian compressive sampling," *IEEE Trans. Antennas Propag.*, vol. 60, no. 5, pp. 2309–2326, May 2012.
- [30] S. E. Nai, W. Ser, Z. L. Yu, and H. Chen, "Beampattern synthesis for linear and planar arrays with antenna selection by convex optimization," *IEEE Trans. Antennas Propag.*, vol. 58, no. 12, pp. 3923–3930, Dec. 2010.
- [31] W. Khawaja, M. Ezuma, V. Semkin, F. Erden, O. Ozdemir, and I. Guvenc, "A survey on detection, classification, and tracking of UAVs using radar and communications systems," *IEEE Commun. Surveys Tuts.*, early access, Mar. 25, 2025, doi: 10.1109/COMST.2025.3554613.
- [32] M. D. Zoltowski and T.-S. Lee, "Beamspace ML bearing estimation incorporating low-angle geometry," *IEEE Trans. Aerosp. Electron. Syst.*, vol. 27, no. 3, pp. 441–458, May 1991.
- [33] D. Park, E. Yang, S. Ahn, and J. Chun, "Adaptive beamforming for low-angle target tracking under multipath interference," *IEEE Trans. Aerosp. Electron. Syst.*, vol. 50, no. 4, pp. 2564–2577, Oct. 2014.
- [34] L. Xu, J. Li, and P. Stoica, "Radar imaging via adaptive MIMO techniques," in *Proc. 14th Eur. Signal Process. Conf.*, Sep. 2006, pp. 1–5.
- [35] Y. Nesterov and A. Nemirovskii, *Interior-Point Polynomial Algorithms in Convex Programming*. Philadelphia, PA, USA: Society for Industrial and Applied Mathematics, 1994. [Online]. Available: <https://epubs.siam.org/doi/abs/10.1137/1.9781611970791>
- [36] G.-H. Ko, J. Y. Park, K.-I. Oh, G. S. Kim, E. Hyun, J.-R. Yang, J.-G. Kim, and D. Baek, "24-GHz 4TX-4RX phased array transceiver with automatic beam steering mode for FMCW radar applications," *IEEE Trans. Microw. Theory Techn.*, vol. 72, no. 5, pp. 3065–3075, May 2024.
- [37] Y. Chen, Y. Liu, Y. Zhang, Z. Yue, and Y. Jia, "A 24 GHz millimeter wave microstrip antenna array for automotive radar," in *Proc. Int. Symp. Antennas Propag. (ISAP)*, Oct. 2019, pp. 1–2.
- [38] H. L. Van Trees, *Optimum Array Processing: Part IV of Detection, Estimation, and Modulation Theory*. Hoboken, NJ, USA: Wiley, 2002.
- [39] P. Stoica, E. G. Larsson, and A. B. Gershman, "The stochastic CRB for array processing: A textbook derivation," *IEEE Signal Process. Lett.*, vol. 8, no. 5, pp. 148–150, May 2001.



**HUIJEA PARK** received the B.S. degree in electronic engineering from Pukyong National University, South Korea, in 2024, where he is currently pursuing the M.S. degree with the Department of Electronic Engineering. His research interests include radar signal processing, FMCW radar systems, 2D MUSIC estimation, IMM filtering, and stepped-carrier OFDM radar. His current work focuses on target tracking and high-resolution parameter estimation using real-world radar measurements.



**JIWON KIM** received the B.S. degree in electronic engineering from Pukyong National University, South Korea, in 2024, where she is currently pursuing the M.S. degree with the Department of Electronic Engineering. Her research interests include radar signal processing based on multiple-input multiple-output (MIMO) antenna systems, with a focus on beamforming and multi-target angle estimation.



**JAEHYUN PARK** (Member, IEEE) received the B.S. and Ph.D. (M.S.–Ph.D. joint program) degrees in electrical engineering from Korea Advanced Institute of Science and Technology (KAIST), in 2003 and 2010, respectively. From 2010 to 2013, he was a Senior Researcher with the Electronics and Telecommunications Research Institute (ETRI), where he worked on transceiver design and spectrum sensing for cognitive radio systems. From 2013 to 2014,

he was a Postdoctoral Research Associate with the Electrical and Electronic Engineering Department, Imperial College London. He is currently a Professor with the Electronic Engineering Department, Pukyong National University, South Korea. His research interests include signal processing for wireless communications and radar systems, with a focus on detection and estimation for MIMO systems, MIMO radar, cognitive radio networks, and joint information and energy transfer.



**JAE CHEOL PARK** received the B.S. degree in electronics engineering and the M.S.E. degree in electronics and radio engineering from Kyung Hee University, in 2009 and 2010, respectively, and the Ph.D. degree in electrical engineering from KAIST, in 2024. He is currently a Principal Researcher with ETRI. His research interests include the design and analysis of UAV communication systems, machine learning for wireless communication systems, and mmWave communication systems.



**JUNGICK MOON** (Member, IEEE) received the M.S. and Ph.D. degrees in electrical engineering from the Department of Electrical Engineering, KAIST, Daejeon, South Korea, in 2000 and 2004, respectively. Since 2004, he has been with ETRI, as a Principal Researcher. His research interests include small and broadband antennas, wireless power transmission, and RF energy harvesting technologies.

...